Theory of $(s + id)$ pairing in mixed-valent correlated metals

Emilian M. Nica* and Onur Erten
Department of Physics, Arizona State University, P.O. Box 871504, Tempe, Arizona 85287-1504, USA

(Received 10 July 2020; revised 8 December 2020; accepted 10 December 2020; published 21 December 2020)

Motivated by the recent discovery of superconductivity in square-planar nickelates as well as by longstanding puzzling experiments in heavy-fermion superconductors, we study Cooper pairing between correlated d electrons coupled to a band of weakly correlated electrons. We perform self-consistent large N calculations on an effective $t - J$ model for the d electrons with additional hybridization. Unlike previous studies of mixed-valent systems, we focus on parameter regimes where both hybridized bands are relevant to determine the pairing symmetry. For sufficiently strong hybridization, we find a robust $(s + id)$ pairing which breaks time-reversal and point-group symmetries in the mixed-valent regime. Our results illustrate how intrinsically multiband systems such as heavy fermions can support a number of highly nontrivial pairing states. They also provide a putative microscopic realization of previous phenomenological proposals of $(s + id)$ pairing and suggest a potential resolution to puzzling experiments in heavy-fermion superconductors such as $U_{1-x}Th_xBe_{13}$ which exhibit two superconducting phase transitions and a full gap at lower temperatures.

DOI: 10.1103/PhysRevB.102.214509

I. INTRODUCTION

The historic search for superconductivity (SC) in Ni-based oxides [1] recently passed an important milestone with Sr-doped $NdNiO_2$ [2–4]. This long-term pursuit in the nickelates has been partly driven by the similarities with the cuprates. Indeed, both nickelates and cuprates are quasi-two-dimensional and share a nominally half-filled $d_{x^2-y^2}$ orbital with $3d^9$ configuration. However, unlike the typical cuprate parent compound, $NdNiO_2$ is a paramagnetic metal [2] instead of an antiferromagnetic insulator, due to the presence of additional Nd d bands that cross the Fermi level. Self-doping effects push the Ni $d_{x^2-y^2}$ band away from half filling [5] and thus from the canonical proximity to the Mott insulator typical of the cuprates. A proper treatment of SC in the nickelates must therefore incorporate the strong correlations of the Ni $d_{x^2-y^2}$ bands and the coupling to weakly interacting Nd d bands alike. In many ways, this parallels heavy-fermion intermetallics [6], where the strongly interacting f states couple to weakly correlated d electrons. Among the intermetallics, actinides with $5f$ orbitals particularly resemble the nickelates since they are closer to the mixed-valent regimes than the lanthanides. They also exhibit superconducting transition temperatures (T_c's) which are comparable to that observed in Sr-doped $NdNiO_2$, as in the case of $PuCoGa_5$ where $T_c \sim 18.5$ K [7].

To investigate the effects of weakly correlated conduction (c) electrons on the Cooper pairing of correlated d electrons, we study a general $t - J_H$ model that includes the usual nearest-neighbor (NN) d-electron hopping t_d and Heisenberg exchange J_H, but which also incorporates a $c - d$ hybridization V, taken to be local for simplicity. We perform large N calculations within a Sp(N) representation of the local moments and find that $(s + id)$ pairing typically occurs in a mixed-valent regime provided that the hybridization is sufficiently strong with $V\sqrt{1 - n_d} \sim J_H$ and $t_d/V \ll 1$, where n_d is the d-electron filling. The emergence of $(s + id)$ pairing is inherently a two-band phenomenon, requiring a multipocketed Fermi surface (FS) with significant d-electron content near the Fermi level for both bands. Figure 1 summarizes our main conclusions. Our results illustrate the importance of nontrivial multiband SC, as noted by several proposals for Fe-based [8–18], heavy-fermion [19–22] SCs, and twisted-bilayer graphene [23,24], as well as by other references cited therein.

$(s + id)$ pairing is highly unusual as it breaks time-reversal symmetry. Furthermore, it also breaks the point-group symmetry since it is a linear combination of two inequivalent irreducible representations of D_{4h}. Consequently, these two channels are not coupled to leading order in a Landau-Ginzburg (LG) theory, and we expect that this type of pairing generally requires two second-order transitions with decreasing temperature. Moreover, $(s + id)$ pairing vanishes at only four points in the entire Brillouin zone (BZ) and we expect that the quasiparticle spectrum is typically completely gapped, although accidental point nodes are possible. While our predictions do not strictly apply to the nickelates, where the hybridization between the Ni and the less correlated Nd is typically small, they can provide insight into a number of puzzling experiments in heavy fermion superconductors. One prominent example is the observation of two superconducting phase transitions into a gapped state in $U_{1-x}Th_xBe_{13}$ [25–28]. Indeed, Kumar and Wolfle proposed an $(s + id)$ state for $U_{1-x}Th_xBe_{13}$ based on a phenomenological LG theory [29], whereas here we provide a concrete, microscopic realization of such a state in a simple, prototypical model for mixed-valent systems. Cubic $U_{1-x}Th_xBe_{13}$ compounds are subject to strong spin-orbit coupling [30], present a complex

*Corresponding author: enica@asu.edu

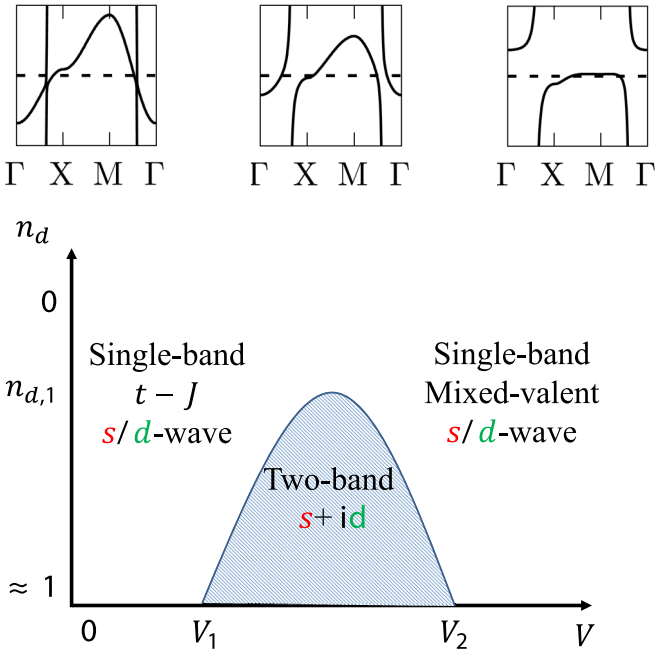

FIG. 1. General phase diagram at zero temperature for $(s+id)$ pairing in a $t-J$ model with a coupling to conduction electrons. V and n_d are the hybridization strength and d-electron filling, respectively. For simplicity, we consider the case where the hybridization is larger than the d-electron hopping $t_d \ll V$. When the hybridization is also much weaker than the Heisenberg exchange $V \ll J_H$, the pairing instability is determined by a single band with predominant d-electron character, as in the $t-J$ model, and the pairing symmetry is typically either s or d wave. In the regime where $V\sqrt{1-n_d} \approx J_H$, both of the hybridized bands have significant d-electron content and $(s+id)$ emerges as the dominant pairing. Our results are consistent with second-order phase transitions at the boundary of this regime, which is bounded by $V_{1/2}$ and $n_{d,1}$. In the large-V limit, a dominant hybridization gap suppresses pairing on the higher-energy band, resulting in a single-band pairing with either s- or d-wave symmetry. The upper panels illustrate the general evolution of the hybridized bands in the normal state with increasing V.

phase-diagram as a function of doping and temperature [31], and exhibit marked non-Fermi liquid behavior in the normal state [32]. A study of pairing in models which take such features into account is therefore very challenging. On the other hand, $(s+id)$ pairing emerges in our controlled approach under quite inclusive conditions, as illustrated in Fig. 1. It is then natural to expect that our results in part illustrate how $(s+id)$ pairing can occur in models which account for the aspects specific to such mixed-valent compounds as $U_{1-x}Th_xBe_{13}$.

In this paper, we focus on the mechanisms which can lead to the emergence of $(s+id)$ pairing in mixed-valent systems rather than an exhaustive study of the phase diagram. In spite of the simplicity of our model, we believe that our main conclusions can also be applied to models with more realistic band structures.

Our paper is organized as follows. We discuss the general mechanism behind $(s+id)$ pairing in Sec. II. In Sec. III, we introduce our model within a Sp(N) representation of the spins, derive the mean-field self-consistency equations and Bogoliubov-de Gennes (BdG) spectrum. Our numerical results for several regimes are presented in Sec. IV. We discuss our main conclusions in Sec. V.

II. $(s+id)$ PAIRING IN A TWO-BAND REGIME

Our model for physical correlated (d) electrons is mapped onto an effective f-fermion model with renormalized parameters within a slave-boson mean-field theoretical approach. The pairing of these f fermions is determined self-consistently via a standard gap equation, in conjunction with remaining mean-field parameters. Hence, the notions of FS and density of states (DOS) defined for the auxiliary f fermions are crucial in understanding why this type of pairing occurs, although they need not have an immediate physical meaning. Similarly, $f-f$ pairing is not a SU(2) gauge-invariant quantity and is thus not a physical observable. The BdG spectrum determined from our effective model is nonetheless physically meaningful. $(s+id)$ pairing for the f fermions typically leads to a gapped BdG spectrum while breaking time-reversal symmetry, features which remain relevant for the model defined in terms of the physical d electron.

To understand how $(s+id)$ emerges in our effective model for the f fermions, we first consider the $t-J$ limit with $V=0$. We define an effective kinetic energy scale which is determined for arbitrary doping by the renormalized hopping $t_d b^2$ and by the contribution of the particle-hole (p-h) channel introduced via the NN Heisenberg exchange terms. $b=\sqrt{1-n_f}$ is the amplitude of the condensed boson in terms of the d-electron filling $n_d = n_f$. We can likewise define a scale associated with the pairing interactions $\sim J_H$. In the *absence* of the effective kinetic terms at half-filling, where $b=0$ and the contribution of the p-h terms can be gauged away, the f band becomes flat, leading to $s_{x^2+y^2}$ and $d_{x^2-y^2}$ pairing channels with identical critical temperature T_c [33], defined via the gap equation and not representing physical SC. Furthermore, $(s+id)$ pairing emerges at zero temperature for $t_d/J_H \lessapprox 1$ within a finite range of hole doping, provided that the p-h contribution to the kinetic energy is ignored [34]. Whenever these p-h terms are taken into account, the quasidegeneracy between s and d waves is lifted, and $(s+id)$ pairing is consequently suppressed [35].

In our model, the hybridization between the d and c electrons introduces an additional scale. In the canonical mixed-valent limit where $t_d, J_H \ll V$, the scale associated with the hybridization is determined essentially by the indirect hybridization gap $\sim(Vb)^2$ [36], as depicted in the right top panel in Fig. 1. Since the indirect gap exceeds both the effective kinetic and pairing ($\sim J_H$) scales, $f-f$ pairing is determined by the single FS due to the lower band [37] and the degeneracy between s or d waves is typically lifted, leading to a suppression of $(s+id)$ pairing. When $(Vb)^2$ determines the lowest scale, we recover the $t-J$ model limit discussed previously. We find that in an intermediate regime where $(Vb)^2$ is comparable to both effective kinetic energy and pairing strength scales or, equivalently, when the FS and f fermion content of both bands are relevant to the pairing instability, $(s+id)$ becomes the preferred state at zero temperature.

$(s+id)$ emerges in these regime via two effects apparent in the normal state for $T > T_c$. First, due to the hybridization,

both c-like and f-like bands support $f-f$ pairing, in contrast to the single-band limits of the $t-J$ and simple mixed-valent cases, respectively. As the hybridization increases, the FS of the f-like band expands while that of the c-like band contracts. The f-like FS remains in the vicinity of the nodes of the $s_{x^2-y^2}$ form factor and thus promotes $d_{x^2-y^2}$ pairing instead. The c-like FS, which is centered on the Γ point, promotes $s_{x^2-y^2}$ since the $d_{x^2-y^2}$ form factor vanishes at (0,0). These two sectors of the FS thus promote two distinct channels, leading to a coexisting $(s+id)$ state. The FS shape here is strongly reminiscent of the Fe pnictides, where FS pockets present at the edges and center of the BZ [16,18] can lead to degenerate $s_{\pm}$ and $d_{x^2-y^2}$ channels. A similar mechanism persists even when the pocket at Γ vanishes with increasing hybridization, provided that the indirect gap remains comparable to the strength of the pairing interactions. Similar effects were noted in early works on SC in Kondo-lattice systems [37,38] as well as in Fe-based SCs [17].

Second, we observe that the f-fermion DOS becomes increasingly concentrated near the Fermi level in the regime where $(s+id)$ pairing dominates. This is partially a natural consequence of increasing hybridization, as the c-like band which overlaps with the f-like band in energy gets pushed to higher energies. However, we also observe an additional effect, as the self-consistent p-h mean-field parameter $K_{\hat{x},\hat{y}}$ is also suppressed with increasing hybridization. This leads to a reduction of the effective kinetic energy, and thus to a flattening of the bands which promotes degenerate s- and d-waves in a way analogous to the $t-J$ model with the p-h channel suppressed [34].

The arguments for $(s+id)$ pairing have been based on the properties of the normal state near the pairing $f-f$ critical temperature T_c. Below T_c, the pairing, p-h contributions as well as all of the remaining self-consistent parameters can change, reflecting the self-consist nature of the calculation [35]. However, we find that whenever the normal state reflects the phenomenology discussed thus far, $(s+id)$ pairing remains the preferred state at zero temperature.

We characterize various regimes via six independent dimensionless parameters, three of which are defined in terms of the bare coupling constants $(t_d, V, t_c)/J_H$, where t_c is the c-electron NN hopping. The remaining parameters reflect temperature T/J_H, and the d-electron and total fillings n_d, $n_{\rm tot}$, respectively. For simplicity, we fix J_H, t_c, and T thereby reducing the number of independent parameters to four. $(s+id)$ generally emerges in the $n_d \lessapprox 1$ regime where the kinetic energy controlled by $\sim t_d(1-n_d)/J_H$ is sufficiently suppressed to allow significant f DOS near the Fermi level. In addition, we find that $V(1-n_d)/J_H$ should approach a value close to unity for both bands to be located near the Fermi level. In this regime, we also find that smaller values of t_d/V are favorable to $(s+id)$, since a larger kinetic energy tends to push the normal state away from the ideal conditions discussed previously. As we illustrate below, while $(s+id)$ requires some amount of tuning, it does emerge for a finite range of dimensionless parameters near d half filling.

III. MODELS AND SOLUTION METHODS

In this section, we present our model and solution method. Mixed-valent systems are typically challenging to model faithfully due to complex multiband structures with different degrees of correlation [27]. Similarly, the mechanisms behind Cooper pairing are generally not well-established [27]. Consequently, we consider simplified models which capture the salient features of some of these materials without obscuring the mechanisms behind $(s+id)$ pairing. Our assumptions include (i) a simple square lattice with tetragonal symmetry, (ii) the presence of a single flavor of weakly correlated conduction c electrons with NN hopping which hybridize to the correlated d electrons together with NN hopping for the latter, (iii) c and d electrons which belong to identical representations of the D_{4h} point group, and (iv) the inclusion of significant NN hopping for the d electrons.

In view of points (ii) and (iii), we consider a *local* $c-d$ hybridization. We define an appropriate $t-J$ model which includes the effects of the strong local Coulomb repulsion via the exclusion of double occupancy for d electrons, NN Heisenberg exchange interactions J_H, and $c-d$ hybridization V. Such models interpolate between single-band $t-J$ and canonical mixed-valent systems, where the dispersion of the correlated d electrons is typically ignored.

We generalize the SU(2) symmetry of the local spin operators to Sp(N) symmetry to obtain a controlled saddle-point solution in the limit of large N [34,39]. We introduce a slave-boson representation, decouple the exchange interaction in both p-h and particle-particle (p-p) channels, and solve these models at saddle-point level *at fixed total filling*. Consequently, the d-electron filling is not fixed *a priori* but is determined self-consistently. The Sp(N) slave-boson approach preserves a SU(2) gauge symmetry and involves three local constraints [40,41]. We work in the gauge where one of the bosons is set to zero, such that these constraints reduce to the usual U(1) gauge symmetry condition [34], together with two additional conditions which suppress *on-site* $f-f$ pairing, as a consequence of the local Coulomb repulsion. These additional constraints can also suppress nonlocal s-wave pairing in a single-band $t-J$ model [41]. In our case, we find that these additional constraints are effective in suppressing the $s_{x^2+y^2}$ component in $(s+id)$ pairing, particularly in the regimes shown in Fig. 1 which approach either $t-J$ or single-band mixed-valent limits. By contrast, we find that their effect is small when the hybridized bands contribute both electron and hole pockets, at the center and edge of the BZ, respectively, thus allowing an extended $s_{x^2+y^2}$ to naturally mitigate the effects of the local Coulomb repulsion. Since $(s+id)$ pairing emerges precisely in this regime, it is likewise not significantly suppressed. Finally, we are interested in solutions which preserve the translational symmetry of the lattice and therefore ignore cases exhibiting phase separation [42].

A. Model

We consider the following $t-J$ model with a local $c-d$ hybridization:

$$H = P_d\Bigg[-2t_d\sum_{\langle ij\rangle,\sigma}(d^\dagger_{i\sigma}d_{j\sigma}+\text{H.c.})+(\epsilon_d-\mu)\sum_{i,\sigma}n_{di\sigma}-t_c\sum_{\langle ij\rangle,\sigma}(c^\dagger_{i\sigma}c_{j\sigma}+\text{H.c.})+(\epsilon_c-\mu)\sum_{i,\sigma}n_{ci\sigma}$$
$$+\sqrt{2}V\sum_{i,\sigma}(d^\dagger_{i\sigma}c_{i\sigma}+\text{H.c.})+\frac{J_H}{2}\sum_{\langle ij\rangle}\left(\boldsymbol{S}_{di}\cdot\boldsymbol{S}_{dj}-\frac{1}{4}n_{di}n_{dj}\right)\Bigg]P_d. \tag{1}$$

P_d is the projection of doubly occupied d-electron states, the i, j indices cover the square lattice, σ represents the spins of the electrons, and $\epsilon_{c/d}$ are on-site energies. Similarly,

$$\boldsymbol{S}_{di}=\frac{1}{2}\sum_{\alpha\beta}d^\dagger_{i\alpha}\boldsymbol{\sigma}_{\alpha\beta}d_{i\beta}, \tag{2}$$

$$n_{di\sigma}=d^\dagger_{i\sigma}d_{i\sigma}, \tag{3}$$

$$n_{di}=\sum_\sigma n_{di\sigma}, \tag{4}$$

are the SU(2) spin, spin-resolved, and total d-electron filling operators, respectively. Analogous definitions hold for the c electrons. The d-electron hopping t_d, $c-d$ hybridization V, and NN Heisenberg interactions J_H have been rescaled for convenience.

The model can be formally derived by projecting out double occupancy within a Hubbard model for the d electrons, while allowing the additional hybridization with the c electrons. Although such a procedure also generates additional Kondo exchange interactions, the latter do not introduce any qualitatively new effects at the saddle-point level considered here, and shall therefore be ignored.

In the limit $V\to 0$, the Hamiltonian in Eq. (1) reduces to a single-band $t-J$ model. In the limit $t_d\to 0$, the Hamiltonian reduces to a standard mixed-valent model with additional exchange interactions and d-electron hopping. For general parameters, H interpolates between these two limits.

Following Refs. [34,39], we generalize the Hamiltonian from SU(2) to symplectic Sp(N) symmetry by promoting all spin indices σ to Sp(N) indices p and by subsequently replacing the Heisenberg exchange interaction with the corresponding expression using Sp(N) generators:

$$\frac{J_H}{2N}\sum_{\langle ij\rangle}\sum_{pq}\sum_{\alpha\beta}\sum_{\gamma\delta}S^{pq}_{\alpha\beta}S^{qp}_{\gamma\delta}d^\dagger_{i\alpha}d_{i\beta}d^\dagger_{j\gamma}d_{j\delta}$$
$$=-\frac{J_H}{N}\sum_{pq}\{d^\dagger_{ip}d_{jp}d^\dagger_{jq}d_{iq}+\tilde{p}\tilde{q}d^\dagger_{i\bar{q}}d^\dagger_{jq}d_{jp}d_{i\bar{p}}\}$$
$$-\frac{J_H}{N}\sum_p d^\dagger_{ip}d_{ip}. \tag{5}$$

The Sp(N) generators are [39]

$$S^{pq}_{\alpha\beta}=\delta^p_\alpha\delta^q_\beta-\tilde{\alpha}\tilde{\beta}\delta^p_{-\beta}\delta^q_{-\alpha}, \tag{6}$$

where the indices $p,q\in[\pm1,\pm N]$ with N even and

$$\tilde{p}=\text{sgn}(p). \tag{7}$$

We rescaled the Heisenberg exchange to obtain a finite contribution in the large N limit. For similar reasons, we rescale $t_d\to t_d/N$ and $V\to V/\sqrt{N}$.

B. Saddle-point solutions in the large-N limit

Following Refs. [40,41], we introduce a slave-boson representation for the d-electron operators with double occupancy projected out:

$$P_d d_{ip}P_d\to b^\dagger_i f_{ip}+a^\dagger_i\tilde{p}f^\dagger_{i\bar{p}}, \tag{8}$$

$$P_d d^\dagger_{ip}d_{ip}P_d\to-(b^\dagger_i b_i+a^\dagger_i a_i), \tag{9}$$

where p is an Sp(N) index, as defined previously. The distinction between the first and second expressions above can be traced to the distinction between the associated Hubbard operators. Note the introduction of two bosons b,a, which are required to preserve the SU(2) gauge symmetry of the Sp(N) formulation. As shown in Refs. [40,41], the Sp(N) slave-boson representation requires three constraints:

$$b^\dagger_i b_i-a^\dagger_i a_i+\sum_p f^\dagger_{ip}f_{ip}=\frac{N}{2}, \tag{10}$$

$$\sum_{p>0}\tilde{p}f^\dagger_p f^\dagger_{\bar{p}}+b^\dagger a=0, \tag{11}$$

$$\sum_{p>0}\tilde{p}f_{\bar{p}}f_p+a^\dagger b=0. \tag{12}$$

We are only concerned with mean-field solutions where the bosons are condensed. As such, we choose a gauge where the expectation values of a_i are set to zero to eliminate the on-site $c-f$ pairing terms which arise due to the introduction of two bosons [40,41]. With this choice, it is straightforward to see that the three constraints reduce to the usual U(1) gauge theory constraint,

$$b^\dagger_i b_i+\sum_p f^\dagger_{ip}f_{ip}=\frac{N}{2}, \tag{13}$$

together with two additional constraints which eliminate *on-site* $f-f$ pairing, as a consequence of the local Coulomb repulsion:

$$\sum_{p>0}\tilde{p}f^\dagger_p f^\dagger_{\bar{p}}=0, \tag{14}$$

$$\sum_{p>0}\tilde{p}f_{\bar{p}}f_p=0. \tag{15}$$

The constraint in Eq. (13) is enforced via a real Lagrange multiplier λ, and the remaining two, which form Hermitian

conjugates of each other, via a complex Lagrange multiplier λ_s.

In addition, we impose a fixed total filling

$$\sum_{i,p}\left(f_{ip}^{\dagger}f_{ip}+c_{ip}^{\dagger}c_{ip}-\frac{n_{\rm tot}}{2}\right)=0, \tag{16}$$

where $0\leqslant n_{\rm tot}\leqslant 4$. This condition is enforced via a chemical potential μ. Recall that, unlike the standard single-band $t-J$ model [34,35], here the d-electron filling $n_{di}=n_{fi}$ is not fixed but is determined self-consistently.

We ignore the density-density interactions present in the original model at SU(2) symmetry [42]. Furthermore, we decouple the NN exchange interactions in Eq. (5) in both p-h and p-p channels via the *dimensionless* parameters

$$K_{i,\boldsymbol{e}}=\frac{1}{N}\sum_{q}\left\langle f^{\dagger}_{\boldsymbol{r}_i+\boldsymbol{e},q}f_{\boldsymbol{r}_i,q}\right\rangle, \tag{17}$$

$$B_{i,\boldsymbol{e}}=\frac{1}{N}\sum_{q}\tilde{q}\left\langle f_{\boldsymbol{r}_i,\bar{p}}f_{\boldsymbol{r}_i+\boldsymbol{e},p}\right\rangle, \tag{18}$$

where $\boldsymbol{e}\in\{\hat{\boldsymbol{x}}a,\hat{\boldsymbol{y}}a\}$ are the NN lattice vectors.

We consider solutions at saddle-point level which preserve the translation symmetry of the lattice. It is convenient to choose a gauge where the condensed boson is real and uniform:

$$\langle b_i^{\dagger}\rangle=\langle b_i\rangle=\left(\sqrt{\frac{N}{2}}\right)b, \tag{19}$$

where b is also independent of the lattice site, as are the p-h and p-p dimensionless parameters defined previously.

The LG action per site is

$$\begin{aligned}f=\sum_{p>0}\Bigg\{\frac{1}{N_s}\sum_{\boldsymbol{k}}\Bigg[&-2T\sum_{m}\ln(\cosh(\beta E_{\boldsymbol{k}m}))+\mathrm{Tr}[h_{\boldsymbol{k}}]\\&+2J_H\sum_{\boldsymbol{e}}[B_{\boldsymbol{e}}^{\dagger}B_{\boldsymbol{e}}+\chi_{\boldsymbol{e}}\chi_{\boldsymbol{e}}^{\dagger}]+\lambda(b^2-1)\\&+\mu n_{\rm tot}+(\epsilon_d-\mu)\Bigg]\Bigg\},\end{aligned} \tag{20}$$

where $\beta=1/T$ and $E_{\boldsymbol{k}m}$ are the eigenvalues of

$$H_{\boldsymbol{k}}=\begin{pmatrix}\hat{h}_{\boldsymbol{k}} & \hat{\Delta}_{\boldsymbol{k}}\\ \hat{\Delta}_{\boldsymbol{k}}^{\dagger} & -\hat{h}_{-\boldsymbol{k}}^{T}\end{pmatrix} \tag{21}$$

in a Nambu basis with spinor $\Psi^T=(c_{\boldsymbol{k}p},f_{\boldsymbol{k}p},c_{-\boldsymbol{k}\bar{p}}^{\dagger},f_{-\boldsymbol{k}\bar{p}}^{\dagger})$. The normal part is given by

$$\hat{h}_{\boldsymbol{k}}=\begin{pmatrix}\epsilon_{\boldsymbol{k}c} & Vb\\ Vb & \epsilon_{\boldsymbol{k}f}\end{pmatrix}, \tag{22}$$

where

$$\epsilon_{\boldsymbol{k}c}=-2t_c\sum_{\boldsymbol{k}}\cos(\boldsymbol{k}\cdot\boldsymbol{e})+[\epsilon_c-\mu], \tag{23}$$

$$\epsilon_{\boldsymbol{k}f}=-2t_db^2\sum_{\boldsymbol{k}}\sum_{\boldsymbol{e}}\cos(\boldsymbol{k}\cdot\boldsymbol{e}), \tag{24}$$

$$\begin{aligned}&-2J_H[K'_{\boldsymbol{e}}\cos(\boldsymbol{k}\cdot\boldsymbol{e})-K''_{\boldsymbol{e}}\sin(\boldsymbol{k}\cdot\boldsymbol{e})]\\&+[\epsilon_d-\mu+\lambda].\end{aligned} \tag{25}$$

As the solutions presented here involve $K''_{\boldsymbol{e}}=0$, we define an effective f-fermion hopping as

$$t_{f,\boldsymbol{e}}=t_db^2+J_HK'_{\boldsymbol{e}}. \tag{26}$$

$t_{f,\boldsymbol{e}}$ defines an *effective kinetic energy scale* as discussed in Sec. II.

The pairing part of $H_{\boldsymbol{k}}$ is determined by

$$\hat{\Delta}_{\boldsymbol{k}}=\begin{pmatrix}0 & 0\\ 0 & \Delta_{\boldsymbol{k}}\end{pmatrix}, \tag{27}$$

where

$$\Delta_{\boldsymbol{k}}=-2J_H\sum_{\boldsymbol{e}}B_{\boldsymbol{e}}\cos(\boldsymbol{k}\cdot\boldsymbol{e})+\lambda_s. \tag{28}$$

We also define the complex dimensionless pairing mean-field parameters corresponding to the $s_{x^2+y^2}$ and $d_{x^2-y^2}$ channels as

$$B_s=B_x+B_y=|B_s|e^{i\phi_s}, \tag{29}$$

$$B_d=B_x-B_y=|B_d|e^{i\phi_d}. \tag{30}$$

The relative phase is defined as

$$\phi_{\rm rel}=\phi_s-\phi_d. \tag{31}$$

Saddle-point solutions are obtained in standard fashion via variation of the self-consistent parameters λ, λ_s, $K_{\boldsymbol{e}}$, $B_{\boldsymbol{e}}$, μ, and b. The self-consistency conditions are given in Eqs. (13)–(18) together with

$$\left[-4t_d\sum_{\boldsymbol{e}}\mathrm{Re}K_{\boldsymbol{e}}+\lambda\right]b+\frac{2V}{N}\sum_{p}\mathrm{Re}\left\langle f_{\boldsymbol{r}_ip}^{\dagger}c_{\boldsymbol{r}_ip}\right\rangle=0. \tag{32}$$

In the $t_d=0$ limit, this equation reduces to the standard mixed-valent case [43]. In the $V=0$ limit, we recognize the condition for boson condensation in a typical $t-J$ model [35].

We obtain self-consistent solutions numerically on a 100×100 square lattice. In practice, we tune the d-electron level ϵ_d with all other parameters fixed such that both b and n_f are determined self-consistently.

C. Quasiparticle spectrum for $(s+id)$ pairing

The spectrum of the BdG Hamiltonian in Eq. (21), which determines the physical quasiparticle spectrum is given by

$$E_{\boldsymbol{k}\pm}=\pm\sqrt{\frac{\epsilon_{\boldsymbol{k}c}^2+\epsilon_{\boldsymbol{k}f}^2+2(Vb)^2+\Delta_{\boldsymbol{k}s}^2+\Delta_{\boldsymbol{k}d}^2\pm\sqrt{\left[\left(\epsilon_{\boldsymbol{k}f}^2-\epsilon_{\boldsymbol{k}c}^2\right)+\Delta_{\boldsymbol{k}s}^2+\Delta_{\boldsymbol{k}d}^2\right]^2+4(Vb)^2[(\epsilon_{\boldsymbol{k}f}+\epsilon_{\boldsymbol{k}c})^2+(\Delta_{\boldsymbol{k}s}+\Delta_{\boldsymbol{k}d})^2]}}{2}}, \tag{33}$$

where we used

$$\Delta_{\boldsymbol{k}} = \Delta_{\boldsymbol{k}s} + i\Delta_{\boldsymbol{k}d}, \tag{34}$$

with $\Delta_{\boldsymbol{k}s/d}$ real. Note the inner square root which is due to the noncommuting matrices $\hat{h}_{\boldsymbol{k}}$ and $\hat{\Delta}_{\boldsymbol{k}}$ defined in Eqs. (22) and (27). Consequently, the gap is not $|\Delta_{\boldsymbol{k}}|^2$ as in a simple one-band case [11]. The spectrum reverts to an effective single-band $t-J$ case when $(Vb)^2 \ll \Delta_{\boldsymbol{k}s}^2 + \Delta_{\boldsymbol{k}d}^2$ with a conventional gap on the f band. Similarly, in the opposite limit $(Vb)^2 \gg \Delta_{\boldsymbol{k}s}^2 + \Delta_{\boldsymbol{k}d}^2$, we recover the spectrum of weak-coupling pairing occurring predominantly on the lower-energy f-like band.

As both $\Delta_{\boldsymbol{k}s/d}$ vanish at $(\pm\pi/2, \pm\pi/2)$, nodes at $E_{\boldsymbol{k}\pm} = 0$ can appear provided that these points are on the FS. More generally, due to the two-band nature of $(s+id)$ pairing, which is reflected in the unconventional form of the gap, it is possible that nodes can emerge away from $\pi/2, \pi/2$ even though $\Delta_{\boldsymbol{k}s}^2 + \Delta_{\boldsymbol{k}d}^2$ remains finite. This is due to the additional inner-square root term in Eq. (33), which can compensate the remaining factors.

IV. RESULTS

We use a convention whereby all coupling constants appearing in our model have arbitrary units of energy. Without loss of generality, we set the c-electron NN TB coefficient t_c and on-site energies ϵ_c to 0.5 and 0, respectively.

We first illustrate the emergence of $(s+id)$ pairing from the $t-J$ limit under increasing the local $c-d$ hybridization V. We present our results for two values of the fixed d-electron hopping $t_d = 0.01$ and 0.1 at fixed total filling $n_{\rm tot} = 1.473$, NN Heisenberg exchange $J_H = 0.0375$, and c-electron NN hopping $t_c = 0.5$, while varying V for a finite range of d-electron filling n_d. We subsequently consider cases with smaller $n_{\rm tot} = 1.16$. Our results illustrate that $(s+id)$ pairing occurs for a set of different parameters and hence that this unconventional pairing state does not require fine-tuning.

As the filling of the physical d electrons coincides with that of the auxiliary f fermions within the slave-boson approximation, i.e., $n_d = n_f$, we shall use the two naming conventions interchangeably. All our results correspond to self-consistent solutions with condensed boson $b \neq 0$.

A. $t_d = 0.01$, $J_H = 0.0375$, and $n_{\rm tot} = 1.473$

We consider the case for $t_d = 0.01$, $J_H = 0.0375$ with fixed $n_{\rm tot} = 1.473$. In this limit, the hopping of the d electrons [see Eq. (26)], plays a subleading role when compared to the contribution of the p-h mean-field parameter K_e. In Fig. 2, we plot the amplitudes of the $d_{x^2-y^2}$ and $s_{x^2+y^2}$, $f-f$ dimensionless pairing mean-field parameters [see Eqs. (29) and (30)], at zero temperature as functions of the hybridization V and filling n_f.

As shown in Fig. 2(a), the d-wave amplitude remains finite throughout the entire range of n_f, although it does suffer a reduction due to the increasing hybridization which pushes the system away from the strong-coupling limit of the $t-J$ model. By contrast, the s-wave amplitude is almost completely suppressed in the $t-J$ limit ($V=0$) (red symbols) but becomes finite for $V \gtrsim 0.15$. To illustrate that the s- and d-wave components are locked into a $(s+id)$ pairing state at

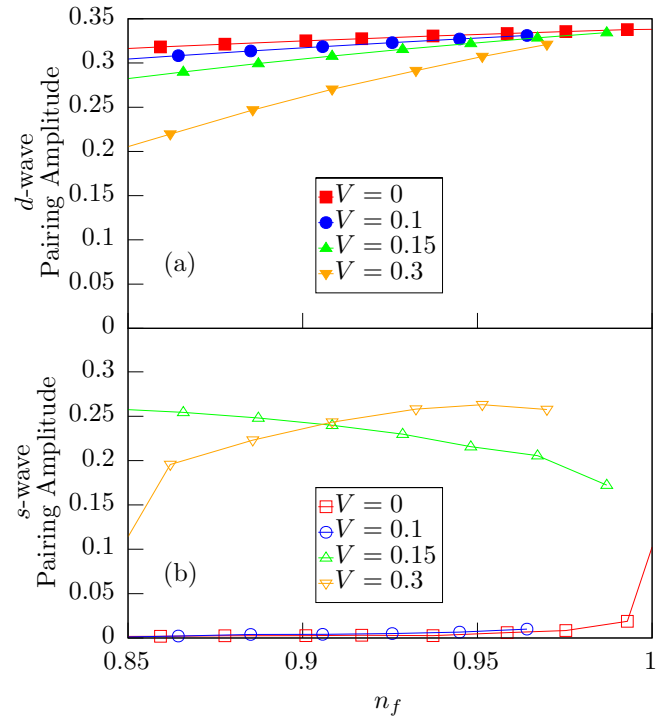

FIG. 2. Amplitudes of the dimensionless $f-f$ pairing amplitudes [Eqs. (30) and (29)] for the $d_{x^2-y^2}$ and $s_{x^2+y^2}$ channels in panels (a) and (b), respectively, as functions of the hybridization V and d-electron filling $n_d = n_f$ for fixed $t_d = 0.01$, $J_H = 0.0375$, and $n_{\rm tot} = 1.473$ at zero temperature. The s-wave amplitude is suppressed in the $t-J$ ($V=0$) limit and becomes finite for $V \gtrsim 0.15$.

$T = 0$, in Fig. 3 we plot the relative phase $\phi_{\rm rel}$ [Eqs. (29) and (30)] of the s- and d-wave channels as functions of V and n_f, modulo π in units of π for a subset of the parameters of Fig. 2. It is apparent that a $\pi/2$ relative phase persists whenever both s- and d-wave amplitudes are finite and therefore, that $(s+id)$ pairing indeed emerges at zero temperature. The $(s+id)$ state persists for larger values of V, albeit within a reduced range of $n_f \approx 1$.

As discussed previously, each of the distinct FS sectors which emerge under increasing hybridization from the $t-J$ limit promote s- and d-waves, respectively. To illustrate this mechanism, we consider the normal state at finite temperature $T = 0.001$ determined from self-consistent solutions with vanishing pairing amplitudes and $b \neq 0$. In Fig. 4, we plot the evolution of the FSs as functions of V for fixed $n_f = 0.9$. At $V = 0$, the larger FS (red solid squares) corresponds to the purely f-fermion band while the smaller pocket (red hollow squares) is comprised entirely of c electrons. As V is increased, the larger pockets (solid symbols) grow and move beyond the diamond shape typical at $n_f = 1$, while the smaller pockets (hollow symbols) shrink and eventually vanish. The s-wave pairing amplitude [Fig. 2(b)] becomes comparable to the d-wave amplitude once the FS moves away from the $(0,\pi)$ to $(\pi,0)$ lines as shown by the green and orange symbols in Fig. 4. We also note that both $V = 0.15$ and $V = 0.3$ cases exhibit comparable s- and d-wave amplitudes although the Fermi pocket at Γ is absent in the latter case. As mentioned previously, this is due to the presence of an indirect gap which

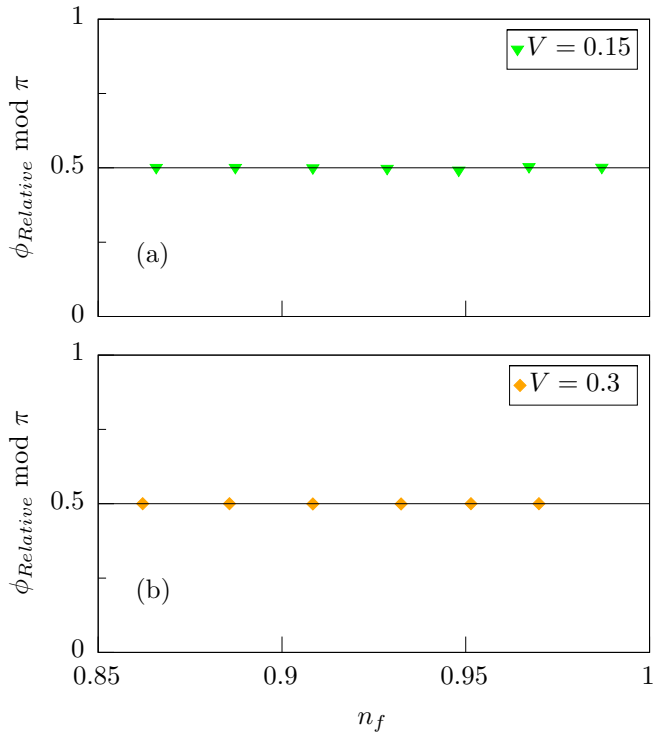

FIG. 3. Relative phase $\phi_{\rm rel}$ [Eqs. (29) and (30)] mudulo π of $s_{x^2+y^2}$ and $d_{x^2-y^2}$ channels as functions of the hybridization V and n_f for fixed $t_d = 0.01, J_H = 0.0375$, and $n_{\rm tot} = 1.473$, at zero temperature in units of π. A $\phi_{\rm rel} = \pi/2$ indicates that s- and d-wave pairing coexist in an $(s + id)$ pairing state.

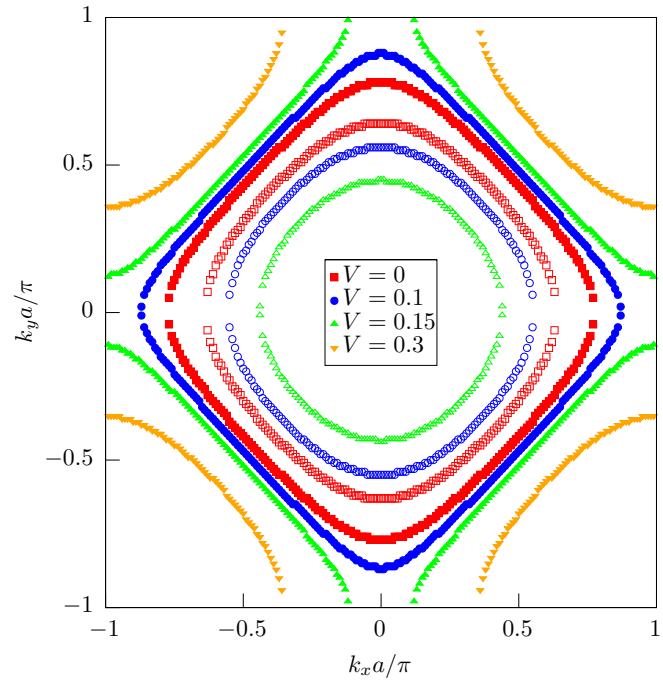

FIG. 4. FSs determined at $T = 0.001$, where the pairing is strongly suppressed, as functions of the hybridization V at fixed $t_d = 0.01, J_H = 0.0375, n_f = 0.9$, and $n_{\rm tot} = 1.473$, covering the same parameter regime of Fig. 2. The red symbols represent the $t - J$ ($V = 0$) limit, with the f fermion and c-electron FSs indicated by the solid and hollow squares, respectively. Increasing V tends to enlarge one of the FS sectors (solid symbols) while shrinking the other (hollow symbols). This change in the FS likewise tends to promote s- and d-wave pairing, as described in the text. Note the absence of the pocket at Γ for $V = 0.3$. Both bands still support $f - f$ pairing, and therefore promote $(s + id)$ pairing, as the indirect gap is smaller than the pairing interactions $\sim J_H$.

is smaller than the pairing interactions $\sim J_H$, ensuring that both bands still support $f - f$ pairing and that they promote s and d waves as in the two-sector FS cases.

Alongside the FS, the f-fermion DOS in the normal state, which reflects the combined contributions of the hopping ($\sim t_d$) and p-h terms ($\sim J_H$) [Eq. (26)] to the effective kinetic energy and the effects of hybridization ($\sim V$), also plays an important role in the emergence of $(s + id)$ pairing. A reduction in the widths of the f DOS peaks promotes degenerate s- and d-wave pairing, as in the $t - J$ model at half filling. To illustrate, in Fig. 5, we plot the f DOS projected onto each of the two bands, in the normal state at $T = 0.001$, as a functions of V, for fixed $t_d = 0.01, J_H = 0.0375, n_f = 0.9$ and $n_{\rm tot} = 1.473$, or in the same parameter regime as Fig. 4. Note that zero-energy corresponds to the Fermi level. A fixed broadening was applied to smoothen the curves. The red solid squares in Fig. 5(a) illustrate the f DOS in the single-band $t - J$ limit. As J_H is the dominant coupling with $t_d/J_H \lessapprox 0.2$ and $V = 0$, the width of the peak is determined mainly by the contribution of the p-h mean-field parameter K_e [Eq. (26)] to the effective kinetic energy. Upon increasing the hybridization to $V = 0.1$, the single peak splits into two contributions for each of the bands, reflecting the mixing of f and c electrons. Most of the f weight still resides in the higher-energy band (solid blue squares). Beyond $V = 0.15$ (green triangles), the weight on the lower-energy band (green hollow triangles) gets shifted closer to the chemical potential at zero energy. Also note the simultaneous change in the FS, as shown in Fig. 4 together with the emergence of $(s + id)$ pairing as shown in Fig. 2(b). The shift in the f DOS closer to the Fermi level together with the change in FSs mark the crossover from effective single-band pairing in the small $V \ll 0.1$ regime to the intermediate two-band pairing picture illustrated in Fig. 1 and discussed in Sec. II. For even higher $V = 0.3$ (orange symbols), we note a dramatic sharpening of the peak for the lower-energy band and a simultaneous opening of a hybridization gap which is slightly obscured by the artificial broadening. The sharp peak can be attributed to the p-h term which *changes sign with respect to* t_d, ensuring an even greater reduction in the effective bandwidth [Eq. (26)]. The reduction in kinetic energy w.r.t the $t - J$ limit, as demonstrated by the narrowing of the f DOS peaks with increasing hybridization promotes degenerate s- and d-wave pairing.

To further illustrate the reduction of the effective kinetic energy with increasing hybridization, in Fig. 6 we plot the amplitude of the dimensionless NN p-h mean-field parameter $|K| = |K_{\hat{x}}| = |K_{\hat{y}}|$ [Eq. (17)] in the normal state at $T = 0.001$, as a function of V and f filling n_f for fixed $t_d = 0.01, J_H = 0.05$, and $n_{\rm tot} = 1.473$. K renormalizes the hopping of the f fermions [Eq. (26)] and thus controls the effective kinetic energy. It is apparent that $|K|$ decreases monotonically for V

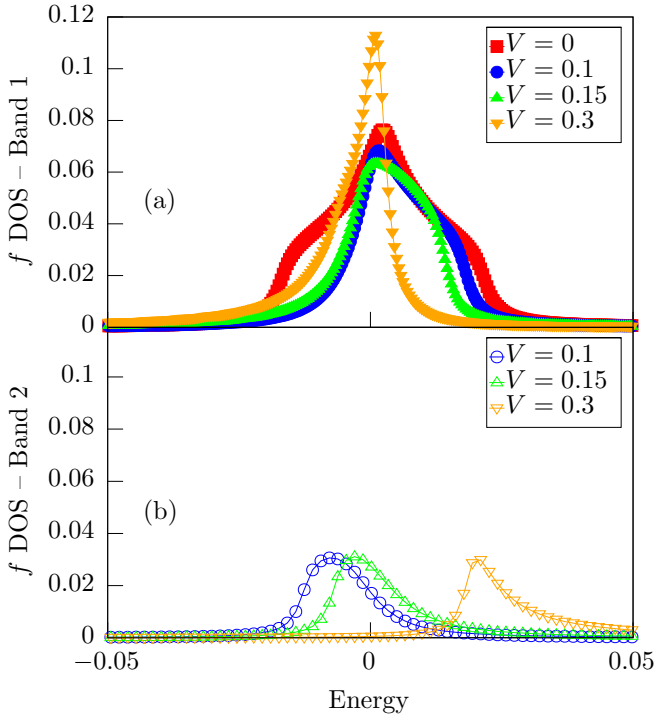

FIG. 5. f DOS in the normal state at $T = 0.001$ projected onto each of the two bands as functions of energy and V at fixed $t_d = 0.01$, $J_H = 0.0375$, $n_f = 0.9$, and $n_{\text{tot}} = 1.473$. A uniform broadening is applied in all cases. The chemical potential is pinned to zero energy. The DOS is illustrated for a single band in the $t - J$ limit (red symbols). A narrowing of the peaks is apparent with increasing V culminating with the $V = 0.3$ case (orange symbols). The dramatic sharpening of the peaks in this case is due to a change in sign of the self-consistent p-h parameter K which strongly renormalizes the kinetic energy due to hopping [$\sim t_d$, Eq. (26)]. The hybridization gap in this case is filled due to the artificial broadening.

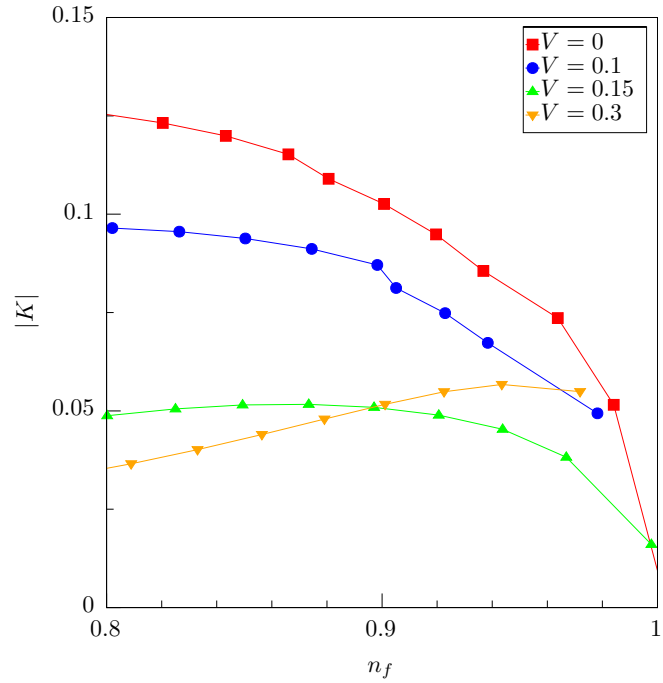

FIG. 6. Amplitudes of the p-h mean-field parameter $|K| = |K_{\hat{x}}| = |K_{\hat{x}}|$ in the normal state at $T = 0.001$ as functions of V and n_f, for fixed $t_d = 0.01$, $J_H = 0.0375$, and $n_{\text{tot}} = 1.473$. $|K|$ decreases with increasing V for $V \leqslant 0.15$. Although $|K|$ increases from $V = 0.15$ to $V = 0.3$, the sign of this mean-field parameter also changes within this range, further reducing the effective kinetic energy in Eq. (26).

up to 0.15. For $V = 0.3$, the amplitude of K actually increases near $n_f \approx 1$. However, in contrast to all of the other cases shown here, K changes sign, and is therefore subtracted from rather than added to the part proportional to t_d. This ensures that the f DOS is strongly peaked near the Fermi level, as shown in Fig. 5.

B. $t_d = 0.1$, $J_H = 0.0375$, and $n_{\text{tot}} = 1.473$

To illustrate that the $(s + id)$ pairing state can occur in a finite range of d-electron filling for larger values of the hopping coefficient t_d, we present our results for $t_d = 0.1$, one order of magnitude larger than previously shown in Sec. IV A, for fixed $J_H = 0.0375$.

In Fig. 7, we show the d- and s-wave pairing amplitudes at $T = 0$ as functions of V and n_f for fixed total filling $n_{\text{tot}} = 1.473$. As for the smaller $t_d = 0.01$, the s-wave amplitude is suppressed in the $t - J$ limit for $V = 0$ shown in Fig. 7(b) (red, hollow squares). However, it becomes finite for $V \geqslant 0.5$. The mechanisms behind the emergence of $(s + id)$ pairing are similar to those for the $t_d = 0.01$ case of Sec. IV A, as shown in the Appendix.

Note that for $V = 0.5$ and for $nf \lessapprox 0.83$, there is a second-order phase transition from $(s + id)$ to simple s wave instead of simple d wave, as for the other values of V shown in Fig. 7. As the f DOS stays relatively constant for a range exceeding the pairing strength $\sim J_H$ in the vicinity of the Fermi level, the pairing falls within a weak-coupling regime as shown in Fig. 13 in the Appendix. The corresponding FS (shown in Fig. 12 of the Appendix) maintains contributions from both bands even in this limit, in contrast to the cases with $t_d = 0.01$ discussed in Sec. IV A. This illustrates that the emergence of $(s + id)$ pairing requires both a sufficiently strong concentration of f DOS states near the Fermi level and a favorable FS.

C. $t_d = 0.1$, $J_H = 0.0375$, and $n_{\text{tot}} = 1.16$

We illustrate that $(s + id)$ also emerges near the f half-filling point for a range of total fillings n_{tot}. In Fig. 8, we plot the s- and d-wave amplitudes at $T = 0$ for fixed $t_d = 0.1$, $J_H = 0.0375$, and $n_{\text{tot}} = 1.16$ as functions of V and n_f. The s-wave amplitude becomes significant near half-filling, although it is suppressed when compared to the results of $n_{\text{tot}} = 1.473$ presented in the previous sections. This suppression is a consequence of the reduced size of the FS pocket at the center of the BZ, as the c band is nearer to its bottom for this regime of smaller total filling. For the same reason, the bare f- and c-bands are nearer in energy such that the hybridization further depletes the f DOS near the Fermi level.

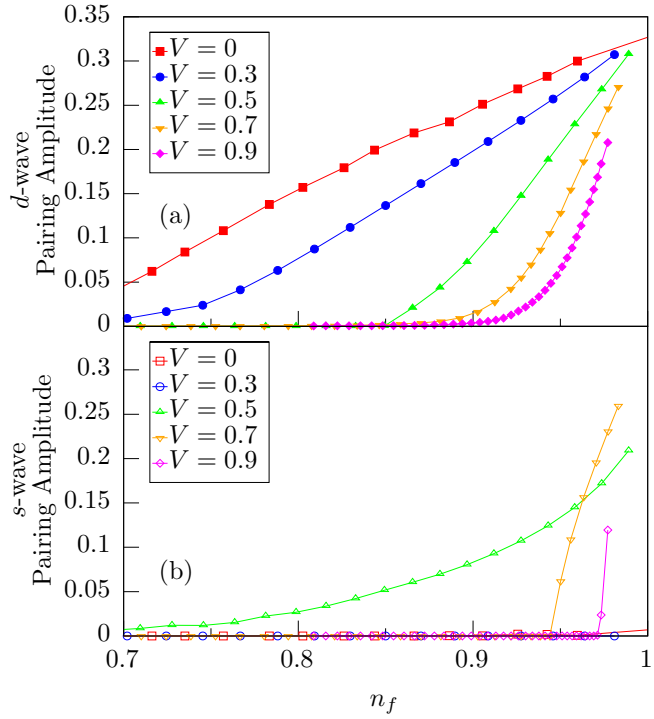

FIG. 7. Amplitudes of the dimensionless $f - f$ pairing amplitudes for the $d_{x^2-y^2}$ and $s_{x^2+y^2}$ channels in panels (a) and (b), respectively, as functions of the hybridization V and n_f for fixed $t_d = 0.1, J_H = 0.0375, n_{\text{tot}} = 1.473$ at zero temperature. The s-wave amplitude is suppressed in the $t - J$ ($V = 0$) limit and becomes finite for $V \geqslant 0.5$. Note that for $V = 0.5$ and smaller n_f, $(s + id)$ pairing is suppressed in favor of a simple s wave.

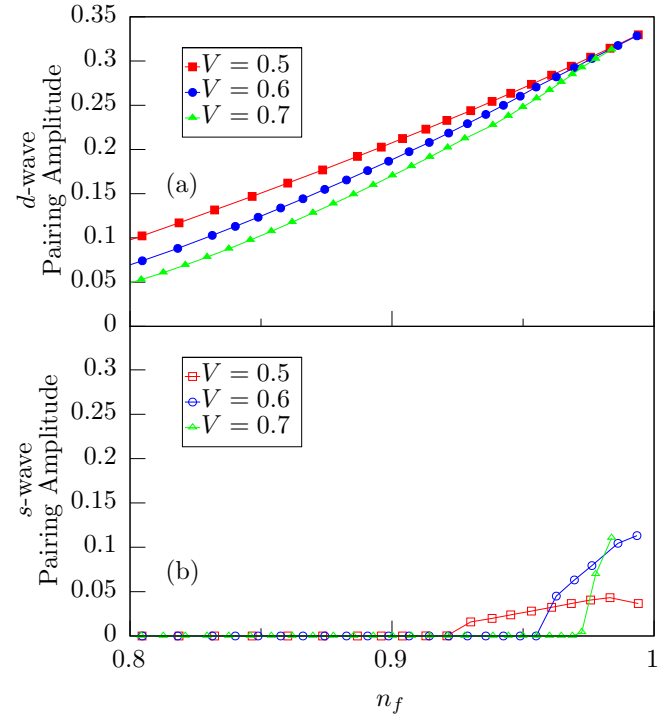

FIG. 8. Amplitudes of the dimensionless $f - f$ pairing amplitudes for the $d_{x^2-y^2}$ and $s_{x^2+y^2}$ channels in panels (a) and (b), respectively, as functions of the hybridization V and n_f for fixed $t_d = 0.1, J_H = 0.0375$, and reduced total filling $n_{\text{tot}} = 1.16$ at zero temperature. The s-wave amplitude is finite near the f half-filling point but is suppressed when compared to the cases of higher $n_{\text{tot}} = 1.473$ previously discussed.

V. DISCUSSION

We studied a simplified $t - J$ model for correlated d-electrons which hybridize with weakly correlated c-electrons within a self-consistent mean-field theory with Sp(N) representation of the spins. We found robust $(s + id)$ pairing extending for a finite range near d-electron half-filling for typical values of d-electron hopping and exchange interactions, provided that the hybridization is sufficiently strong to tune the system to an intermediate, two-band pairing regime, as summarized in Fig. 1. We illustrated that the $(s + id)$ state in our model is due essentially to a two-band pairing in contrast to previous studies of $t - J$ models where this type of pairing also emerges under doping.

Our model bridges the gap between two, well-studied limits, corresponding to the effectively single-band $t - J$ model and conventional mixed-valent cases, respectively, as illustrated in Fig. 1. For the d electron near half-filling, the two limits are distinguished by the degree of d-electron delocalization via hybridization with the c electrons. A general measure of the latter is a Kondo temperature scale. In the effective $t - J$ model limit, a small $c - d$ hybridization ensures that the d electrons remain almost localized near half filling, with most of the d-electron spectral weight concentrated on one of the FS sheets. Near half filling, the Heisenberg exchange interaction provides the dominant scale in the system. Conversely, in the more conventional mixed-valent limit, a large $c - d$ hybridization gap ensures that only one of the bands contributes to the FS, leading to either s- or d-wave pairing. The effects of a large hybridization gap on the pairing can in principle be mitigated by very large pairing interactions or, equivalently, by a proportionately large Heisenberg exchange. Therefore, in this limit, the Kondo temperature scale is dominant. The intermediate regime, where both bands contribute to the FS and where $(s + id)$ pairing is dominant, naturally corresponds to a region in phase space where the two scales are comparable.

The importance of the shape of the FS for the stability of a $(s + id)$ pairing phase for weak pairing interactions has been pointed out in the context of Fe-based SCs [16,18]. Our results illustrate that the shape of the FS continues to play an important role when the Kondo and Heisenberg scales are introduced. However, in contrast to the previous proposals, both of these additional scales are already relevant to the emergence of the normal-state properties and the associated FSs which are conducive to $(s + id)$ pairing. In turn, this suggests that $(s + id)$ pairing might provide a viable candidate for a broader class of correlated materials, which can be placed in the intermediate regime illustrated in Fig. 1.

Relevant experimental probes for $(s + id)$ pairing in mixed-valent systems are *a priori* those which can determine the degree of d-electron localization, as previously discussed. Estimates of the Kondo temperature and of the $d - d$ Heisenberg interactions can indicate whether the system is closer to

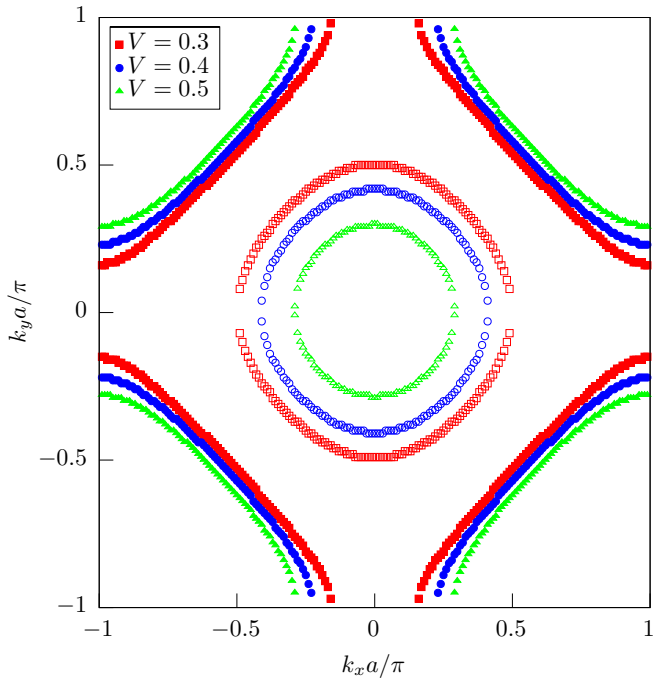

FIG. 9. FSs determined in the normal state at $T = 0.001$ as functions of V for fixed $t_d = 0.1$, $J_H = 0.0375$, $n_f = 0.9$, and $n_{\text{tot}} = 1.473$. The solid symbols are adiabatically connected to the d- and c-electron bands in the $V = 0$ limit. The FSs evolve with increasing V in a way analogous to the cases with smaller $t_d = 0.01$ shown in Fig. 4.

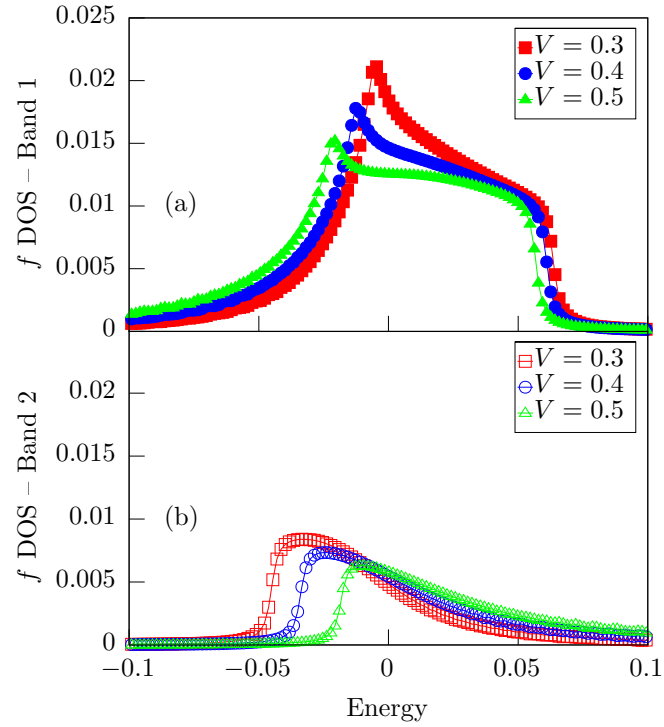

FIG. 10. f DOS projected onto the two bands determined in the normal state $T = 0.001$ as functions of energy and V for fixed $t_d = 0.1$, $J_H = 0.0375$, $n_f = 0.9$, and $n_{\text{tot}} = 1.473$. The Fermi level is pinned to zero energy. The narrowing of the peaks observed for $t_d = 0.01$ in Fig. 5 is obscured here by the much larger value of $t_d = 0.1$.

a typical $t - J$ model or mixed-valent limiting cases, corresponding to a Kondo scale which is the smaller or larger of the two, respectively. These two scales can be estimated via a number of standard experiments which probe the normal-state quasiparticles and the magnetic response, viz., specific heat, transport, susceptibility, and inelastic neutron scattering among others. Provided that the system is in this intermediate regime, ARPES experiments can indicate if the FS is conducive to $(s + id)$ pairing. In addition, experimental probes such as muon-spin spectroscopy and magneto-optical Kerr effect can determine if time-reversal symmetry is broken.

The rather inclusive conditions leading to the emergence of $(s + id)$ pairing within our toy model are possible within more realistic treatments of mixed-valent systems such as DFT + DMFT, provided that the multiband nature of these systems is taken into account. We believe that our results also illustrate how previous phenomenological proposals, as in the case of $U_{1-x}Th_xBe_{13}$, can be realized microscopically within a generic two-band model.

Note added. Recently, we became aware of Refs. [44,45], which consider similar $t - J$ models with additional Kondo interactions in the context of Sr-doped $NdNiO_2$. In Ref. [45], the authors find an $(s + id)$ pairing phase within a renormalized mean-field theory in a regime where the Kondo coupling is the highest energy scale and the Kondo-induced hybridization is finite. In this context, we also note the recent single particle tunneling experiments on superconducting nickelate thin films [46] which find spectra consistent with two distinct pairing symmetries, one which is naturally associated with a d

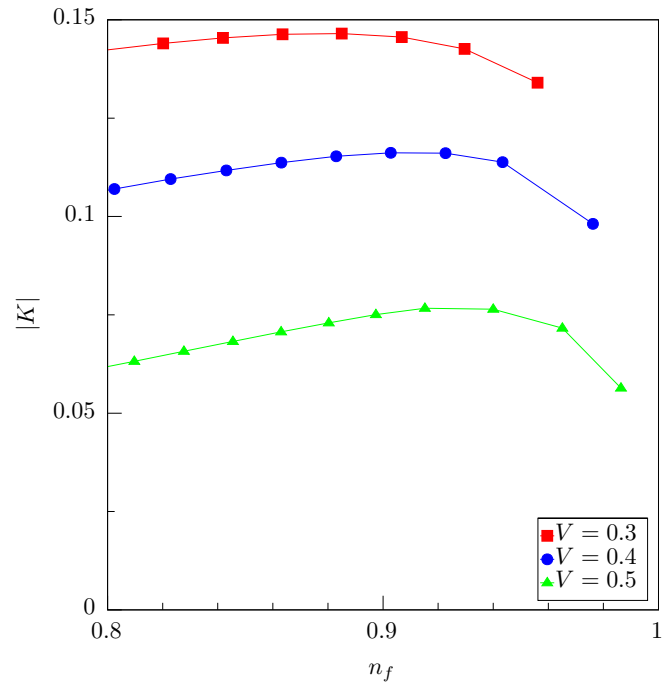

FIG. 11. Amplitudes of the self-consistent p-h terms in the normal state at $T = 0.001$ as functions of V and n_f for fixed $t_d = 0.1$, $J_H = 0.0375$, and $n_{\text{tot}} = 1.473$. The amplitudes decrease monotonically with V.

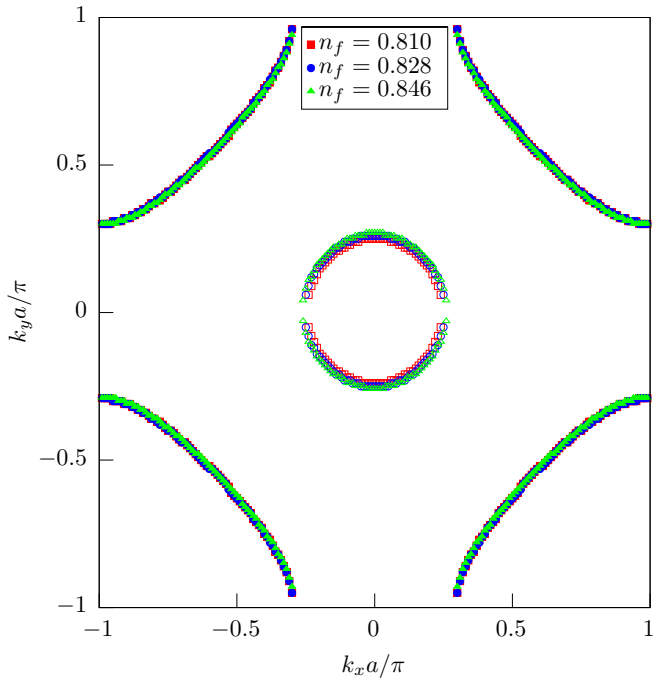

FIG. 12. FSs determined in the normal state at $T = 0.001$ as functions of n_f for fixed $t_d = 0.1, J_H = 0.0375, V = 0.5$, and $n_{\text{tot}} = 1.473$. The FSs remain essentially unchanged within the range of n_f, although the pairing at zero-temperature undergoes a second-order transition from s to $(s + id)$.

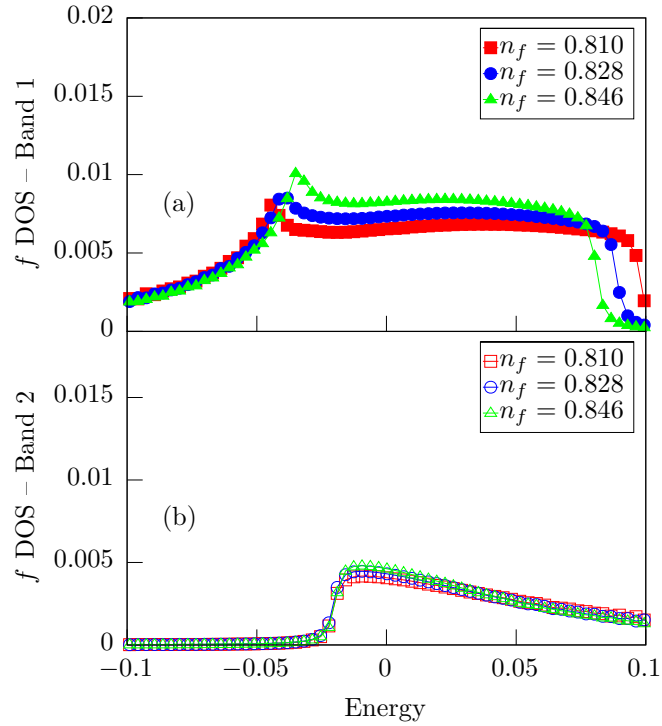

FIG. 13. f DOS in the normal state at $T = 0.001$ as functions of energy and n_f for fixed $t_d = 0.1, J_H = 0.0375, n_{\text{tot}} = 1.473$, and $V = 0.5$. A second-order transition between s wave and $(s + id)$ occurs at zero-temperature across this range of n_f.

wave and another which exhibits a full gap. While tentative at this stage, we find that these studies further hint at the possibility that nontrivial pairings such as $(s + id)$ are not uncommon in systems with pronounced mixed-valent character.

ACKNOWLEDGMENTS

We thank Sumilan Banerjee and Qimiao Si for useful discussions related to this work. E.N. is supported by ASU startup grant and O.E. is supported by NSF-DMR-1904716. We acknowledge the ASU Research Computing Center for HPC resources.

APPENDIX: NORMAL STATE FOR $t_d = 0.1, J_H = 0.0375$ AND $n_{\text{tot}} = 1.473$

In this Appendix, we present the normal-state properties for the case with fixed $t_d = 0.1, J_H = 0.0375$, and $n_{\text{tot}} = 1.473$ discussed in Sec. IV B.

In Fig. 9, we present the FSs determined at $T = 0.001$ and $n_f = 0.9$ as functions of V. Upon increasing V, we observe that the sectors closer to the M points (solid symbols) are growing while those centered on the Γ point are shrinking, mirroring the case with $t_d = 0.01$ shown in Fig. 4.

In Fig. 10, we show the f DOS projected onto the two bands for the same parameter range. We observe a gradual shift in the DOS of band 2 toward the Fermi level at zero-energy with increasing hybridization. Note that the sharpening of the peaks for $t_d = 0.01$ (Fig. 5) which occurs due to a renormalization of the p-h term is obscured here by the much larger contribution of $t_d = 0.1$ to the effective kinetic energy scale although the amplitude of the p-h term is suppressed here as well, as shown in Fig. 11.

In Fig. 12, we show the evolution of the FSs determined in the normal state at $T = 0.001$ as functions of n_f, for fixed $t_d = 0.1, J_H = 0.0375, n_{\text{tot}} = 1.473$, and $V = 0.5$. At zero-temperature there is a second-order phase transition from s-wave to $(s + id)$ pairing with increasing n_f. It is apparent that the FS does not significantly change, indicating that an additional change in the f content of the bands is required for the emergence of this type of pairing.

The corresponding f DOS is shown in Fig. 13. There, the increase in the f DOS near the Fermi level at zero energy, together with a narrowing in the peaks, is apparent for increasing n_f.

[1] S. Middey, J. Chakhalian, P. Mahadevan, J. W. Freeland, A. J. Millis, and D. D. Sarma, Physics of ultrathin films and heterostructures of rare-earth nickelates, Annu. Rev. Mater. Res. **46**, 305 (2016).

[2] D. Li, K. Lee, B. Y. Wang, M. Osada, S. Crossley, H. R. Lee, Y. Cui, Y. Hikita, and H. Y. Hwang, Superconductivity in an infinite-layer nickelate, Nature **572**, 624 (2019).

[3] G. A. Sawatzky, Superconductivity seen in a non-magnetic nickel oxide, Nature **572**, 592 (2019).

[4] S. Zeng, C. Sin Tang, X. Yin, C. Li, Z. Huang, J. Hu, W. Liu, G. Ji Omar, H. Jani, Z. Shiuh Lim, K. Han, D. Wan, P. Yang, A. T. S. Wee, and A. Ariando, Phase Diagram and Superconducting Dome of Infinite-Layer $Nd_{1-x}Sr_xNiO_2$ Thin Films, Phys. Rev. Lett. **125**, 147003 (2020).

[5] M. Hepting, D. Li, C. J. Jia, H. Lu, E. Paris, Y. Tseng, X. Feng, M. Osada, E. Been, Y. Hikita, Y. D. Chuang, Z. Hussain, K. J. Zhou, A. Nag, M. Garcia-Fernandez, M. Rossi, H. Y. Huang, D. J. Huang, Z. X. Shen, T. Schmitt, H. Y. Hwang, B. Moritz, J. Zaanen, T. P. Devereaux, and W. S. Lee, Electronic structure of the parent compound of superconducting infinite-layer nickelates, Nat. Mater. **19**, 381 (2020).

[6] Q. Si and F. Steglich, Heavy fermions and quantum phase transitions, Science **329**, 1161 (2010).

[7] N. J. Curro, T. Caldwell, E. D. Bauer, L. A. Morales, M. J. Graf, Y. Bang, A. V. Balatsky, J. D. Thompson, and J. L. Sarrao, Unconventional superconductivity in $PuCoGa_5$, Nature **434**, 622 (2005).

[8] R. Yu, J.-X. Zhu, and Q. Si, Orbital-selective superconductivity, gap anisotropy, and spin resonance excitations in a multiorbital t-J_1-J_2 model for iron pnictides, Phys. Rev. B **89**, 024509 (2014).

[9] Z. P. Yin, K. Haule, and G. Kotliar, Spin dynamics and orbital-antiphase pairing symmetry in iron-based superconductors, Nat. Phys. **10**, 845 (2014).

[10] T. Ong, P. Coleman, and J. Schmalian, Concealed d-wave pairs in the s± condensate of iron-based superconductors, Proc. Nat. Acad. Sci. **113**, 5486 (2016).

[11] E. M. Nica, R. Yu, and Q. Si, Orbital-selective pairing and superconductivity in iron selenides, npj Quantum Mater. **2**, 24 (2017).

[12] A. Kreisel, B. M. Andersen, P. O. Sprau, A. Kostin, J. C. Seamus Davis, and P. J. Hirschfeld, Orbital selective pairing and gap structures of iron-based superconductors, Phys. Rev. B **95**, 174504 (2017).

[13] H. Hu, R. Yu, E. M. Nica, J.-X. Zhu, and Q. Si, Orbital-selective superconductivity in the nematic phase of FeSe, Phys. Rev. B **98**, 220503(R) (2018).

[14] C. Zhang, R. Yu, Y. Su, Y. Song, M. Wang, G. Tan, T. Egami, J. A. Fernandez-Baca, E. Faulhaber, Q. Si, and P. Dai, Measurement of a Double Neutron-Spin Resonance and an Anisotropic Energy Gap for Underdoped Superconducting $NaFe_{0.985}Co_{0.015}$ as Using Inelastic Neutron Scattering, Phys. Rev. Lett. **111**, 207002 (2013).

[15] P. O. Sprau, A. Kostin, A. Kreisel, A. E. Böhmer, V. Taufour, P. C. Canfield, S. Mukherjee, P. J. Hirschfeld, B. M. Andersen, and J. C. S. Davis, Discovery of orbital-selective Cooper pairing in FeSe, Science **357**, 75 (2017).

[16] W.-C. Lee, S.-C. Zhang, and C. Wu, Pairing State with a Time-Reversal Symmetry Breaking in FeAs-Based Superconductors, Phys. Rev. Lett. **102**, 217002 (2009).

[17] P. Goswami, P. Nikolic, and Q. Si, Superconductivity in multi-orbital $t-J_1-J_2$ model and its implications for iron pnictides, Europhys. Lett. **91**, 37006 (2010).

[18] C. Platt, R. Thomale, C. Honerkamp, S.-C. Zhang, and W. Hanke, Mechanism for a pairing state with time-reversal symmetry breaking in iron-based superconductors, Phys. Rev. B **85**, 180502(R) (2012).

[19] D. F. Agterberg, V. Barzykin, and L. P. Gor'kov, Conventional mechanisms for exotic superconductivity, Phys. Rev. B **60**, 14868 (1999).

[20] G. Pang, M. Smidman, J. Zhang, L. Jiao, Z. Weng, E. M. Nica, Y. Chen, W. Jiang, Y. Zhang, W. Xie, H. S. Jeevan, H. Lee, P. Gegenwart, F. Steglich, Q. Si, and H. Yuan, Fully gapped d-wave superconductivity in $CeCu_2Si_2$, Proc. Nat. Acad. Sci. **115**, 5343 (2018).

[21] E. M. Nica and Q. Si, Multiorbital singlet pairing and d+d superconductivity, arXiv:1911.13274.

[22] M. Smidman, O. Stockert, J. Arndt, G. M. Pang, L. Jiao, H. Q. Yuan, H. A. Vieyra, S. Kitagawa, K. Ishida, K. Fujiwara, T. C. Kobayashi, E. Schuberth, M. Tippmann, L. Steinke, S. Lausberg, A. Steppke, M. Brando, H. Pfau, U. Stockert, P. Sun, S. Friedemann, S. Wirth, C. Krellner, S. Kirchner, E. M. Nica, R. Yu, Q. Si, and F. Steglich, Interplay between unconventional superconductivity and heavy-fermion quantum criticality: $CeCu_2Si_2$ versus $YbRh_2Si_2$, Philos. Mag. **98**, 2930 (2018).

[23] Y.-Z. You and A. Vishwanath, Superconductivity from valley fluctuations and approximate SO(4) symmetry in a weak coupling theory of twisted bilayer graphene, npj Quantum Mater. **4**, 16 (2019).

[24] Y. Su and S.-Z. Lin, Pairing symmetry and spontaneous vortex-antivortex lattice in superconducting twisted-bilayer graphene: Bogoliubov-de Gennes approach, Phys. Rev. B **98**, 195101 (2018).

[25] E.-W. Scheidt, T. Schreiner, P. Kumar, and G. R. Stewart, Specific heat study in $U_{1-x}Th_xBe_{13}$: Enormous ΔC and strong coupling at $x = x_{c1}$ and x_{c2}; Correlation between γ and unusual superconductivity, Phys. Rev. B **58**, 15153 (1998).

[26] B. D. White, J. D. Thompson, and M. B. Maple, Unconventional superconductivity in heavy-fermion compounds, Physica C **514**, 246 (2015).

[27] G. R. Stewart, Unconventional superconductivity, Adv. Phys. **66**, 75 (2017).

[28] G. R. Stewart, UBe_{13} and $U_{1-x}Th_xBe_{13}$: Unconventional superconductors, J. Low. Temp. Phys. **195**, 1 (2019).

[29] P. Kumar and P. Wolfle, Two-Component Order-Parameter Model for Pure and Thorium-Doped Superconducting UBe_{13}, Phys. Rev. Lett. **59**, 1954 (1987).

[30] D. L. Cox and B. Maple, Electronic pairing in exotic superconductors, Phys. Today **48**(2), 32 (1995).

[31] M. Sigrist and K. Ueda, Phenomenological theory of unconventional superconductivity, Rev. Mod. Phys. **63**, 239 (1991).

[32] G. R. Stewart, Non-fermi-liquid behavior in d- and f-electron metals, Rev. Mod. Phys. **73**, 797 (2001).

[33] G. Kotliar, Resonating valence bonds and d-wave superconductivity, Phys. Rev. B **37**, 3664 (1988).

[34] S. Sachdev and N. Read, Large N expansion for frustrated and doped quantum antiferromagnets, Int. J. Mod. Phys. B **5**, 219 (1991).

[35] G. Kotliar and J. Liu, Superexchange mechanism and d-wave superconductivity, Phys. Rev. B **38**, 5142 (1988).

[36] P. S. Riseborough and J. M. Lawrence, Mixed valent metals, Rep. Prog. Phys. **79**, 084501 (2016).

[37] P. Coleman and N. Andrei, Kondo-stabilised spin liquids and heavy fermion superconductivity, J. Phys.: Condens. Matter **1**, 4057 (1989).

[38] N. Andrei and P. Coleman, Cooper Instability in the Presence of a Spin Liquid, Phys. Rev. Lett. **62**, 595 (1989).

[39] R. Flint, M. Dzero, and P. Coleman, Heavy electrons and the symplectic symmetry of spin, Nat. Phys. **4**, 643 (2008).

[40] R. Flint, A. H. Nevidomskyy, and P. Coleman, Composite pairing in a mixed-valent two-channel Anderson model, Phys. Rev. B **84**, 064514 (2011).

[41] R. Flint and P. Coleman, Symplectic-n $t - j$ model and $s_{\pm}$ superconductors, Phys. Rev. B **86**, 184508 (2012).

[42] M. Vojta, Y. Zhang, and S. Sachdev, Competing orders and quantum criticality in doped antiferromagnets, Phys. Rev. B **62**, 6721 (2000).

[43] P. Coleman, Mixed valence as an almost broken symmetry, Phys. Rev. B **35**, 5072 (1987).

[44] G.-M. Zhang, Y.-f. Yang, and F.-C. Zhang, Self-doped Mott insulator for parent compounds of nickelate superconductors, Phys. Rev. B **101**, 020501(R) (2020).

[45] Z. Wang, G.-M. Zhang, Y.-f. Yang, and F.-C. Zhang, Distinct pairing symmetries of superconductivity in infinite-layer nickelates, Phys. Rev. B **102**, 220501(R) (2020).

[46] Q. Gu, Y. Li, S. Wan, H. Li, W. Guo, H. Yang, Q. Li, X. Zhu, X. Pan, Y. Nie, and H.-H. Wen, Two superconducting components with different symmetries in $Nd_{1-x}Sr_xNiO_2$ films, Nat. Commun. **11**, 6027 (2020).